Jpn. J. Appl. Phys. Vol. 41 (2002) pp. 1143–1149
Part 1, No. 2B, February 2002

DC and High Frequency Characterization of Metalorganic Chemical Vapor Deposition (MOCVD) Grown InP/InGaAs PNP Heterojunction Bipolar Transistor

Delong CUI, Shawn S. H. HSU and Dimitris PAVLIDIS*
Department of Electrical Engineering and Computer Science, The University of Michigan, Ann Arbor, MI 48104, USA

(Received June 25, 2001; accepted for publication October 12, 2001)

InP/InGaAs PNP heterojunction bipolar transistor (HBT) layers have been grown by metalorganic chemical vapor deposition (MOCVD) and devices have been fabricated using a self-aligned processing technology. A zinc-doped InP layer has been employed as the wide-bandgap emitter layer for the PNP HBT. The base layer used a 500 Å thick n-type InGaAs layer doped at $5 \times 10^{18}\,\mathrm{cm}^{-3}$. Successful high frequency operation of these devices has been demonstrated. A single-emitter $1 \times 20\,\mu\mathrm{m}^2$ MOCVD-grown PNP InP/InGaAs HBT achieved current gain cutoff frequency (f_T) of more than 11 GHz at a current density (J_C) of $8.25 \times 10^4\,\mathrm{A/cm}^2$. [DOI: 10.1143/JJAP.41.1143]

KEYWORDS: PNP, InP, InGaAs, HBT, MOCVD

1. Introduction

InP-based PNP heterojunction bipolar transistors (HBTs) provide integration possibilities with their NPN counterparts, which have demonstrated extraordinary high frequency operation and high current handling abilities.[1–7] Although PNP HBTs are inherently inferior to their NPN HBT counterparts due to the slower hole than electron transport characteristics, these devices find still a wide range of applications, particularly as monolithic integrated complementary InP NPN-PNP HBT amplifiers.[8] Circuits employing complementary HBT technology include push-pull power amplifier to improve the efficiency and linearity.[9,10] PNP HBTs could also be used to implement active loads for NPN HBTs in order to save in space compared to what is occupied by large value resistors.

GaAs-based PNP HBTs have been studied extensively over the years. Due to the maturity of GaAs-based technology, the best PNP HBT performance was achieved using an AlGaAs/GaAs material design. A cut-off frequency (f_T) of 33 GHz and maximum frequency of oscillation (f_{max}) of 66 GHz were demonstrated by an $Al_{0.4}Ga_{0.6}As$/GaAs HBT design with 325 Å, $7 \times 10^{19}\,\mathrm{cm}^{-3}$ base and 2300 Å $7 \times 10^{16}\,\mathrm{cm}^{-3}$ collector.[11]

InP-based PNP HBT research and development has been mainly concentrated on HBTs employing InAlAs as emitters. The best InAlAs/InGaAs PNP HBTs achieved $\beta = 13$, $f_T = 12\,\mathrm{GHz}$, $f_{max} = 35\,\mathrm{GHz}$[12] and $\beta = 26$, $f_T = 19\,\mathrm{GHz}$ and $f_{max} = 27\,\mathrm{GHz}$.[13] The HBT designs had base layers uniformly doped to $5 \times 10^{18}\,\mathrm{cm}^{-3}$ with base thickness of 500 Å and 350 Å respectively. Other results included DC performance for InAlAs/InGaAs/InAlAs DHBTs with $\beta = 70$ and $BV_{CEO} = 12\,\mathrm{V}$.[14,15] A HBT design with 330 Å, $7 \times 10^{18}\,\mathrm{cm}^{-3}$ base and graded base-emitter junction demonstrated $\beta = 170$, $f_T = 14\,\mathrm{GHz}$ and $f_{max} = 22\,\mathrm{GHz}$.[16]

The only previous report on PNP InP/InGaAs HBTs, as to our knowledge, was by Lunardi *et al.*[17] The HBT layers for the reported device were grown by metalorganic molecular beam epitaxy (MOMBE) and employed a 600 Å, $5 \times 10^{18}\,\mathrm{cm}^{-3}$ base layer. Devices made on these layers demonstrated $\beta = 20$, $f_T = 11\,\mathrm{GHz}$ and $f_{max} = 25\,\mathrm{GHz}$.[17] A first report on metalorganic chemical vapor deposition (MOCVD) grown PNP HBT layers was recently made by the authors.[18] The work reported here provided further details on the design, growth, material, and device properties of PNP InP/InGaAs HBTs grown by MOCVD.

2. MOCVD Growth of PNP InP/InGaAs HBTs

All the material growth done in this study was carried out in a modified EMCORE GS3200 low-pressure metal organic vapor deposition (MOCVD) system. The stainless steel reactor was constructed in a vertical configuration. The carrier gas is H_2 purified by a palladium cell. For all the material growth experiments carried out in this study, the chamber pressure was maintained at 60 Torr.

The PNP InP/InGaAs HBT structure is shown in Fig. 1. It is composed of a 5000 Å p^+-InGaAs subcollector, 3000 Å p^--InGaAs collector, 500 Å n^+-InGaAs base, 100 Å undoped InGaAs spacer, 1500 Å P-InP and 700 Å P^+-InP as emitter, and a 2000 Å p^+-InGaAs emitter cap layer.

The nominal n-type base doping concentration is $5 \times 10^{18}\,\mathrm{cm}^{-3}$. Notice that this value is relative low compared to the typical p-type base doping concentration of a NPN transistor ($2 \times 10^{19}\,\mathrm{cm}^{-3}$), This is due to the fact that lower base resistance can be achieved using n-type material than using p-type material because of the superior electron transport characteristics. Moreover, due to the slower hole transit time in the base, it is necessary to use lower base doping concentration for PNP transistors to ensure a higher current gain.

The growth was carried out at a growth temperature of 570°C. DeZn and Si_2H_6 were used as p-type and n-type dopants respectively. The key for PNP layer growth was to

Layer	Type	Thickness (Å)
Emitter Cap	p^+-InGaAs	2000
	P^+-InP	700
Emitter	P-InP	1500
Spacer	i-InGaAs	100
Base	n^+-InGaAs	500
Collector	p^--InGaAs	3000
Subcollector	p^+-InGaAs	5000
Substrate	Semi-Insulating InP (001)	

Fig. 1. Layer structure of PNP InP/InGaAs HBTs grown by MOCVD.

*E-mail address: pavlidis@umich.edu

achieve high doping concentration for InGaAs subcollector and obtain low doping concentration for the collector layer. In the present MOCVD growth system, the p-type doping range when using DEZn was $1 \times 10^{18}\,\mathrm{cm}^{-3}$ to $2 \times 10^{19}\,\mathrm{cm}^{-3}$. While the highest doping concentration is enough for subcollector and emitter cap doping, the limited minimum doping concentration ($1 \times 10^{18}\,\mathrm{cm}^{-3}$) could degrade the HBT performance as will be described later. Moreover, it is well known that the incorporation efficiency of zinc into InGaAs is 5 to 10 times higher than into InP. Therefore, zinc tends to diffuse through InP into the n^+ InGaAs base. This could also result in the degradation of HBT performance.

Degradation of device performance due to zinc diffusion from base into emitter has been observed in NPN InP/InGaAs HBTs.[19,20] To prevent the zinc diffusion from base to emitter in a NPN transistor, low growth temperature (550°C) was found to be effective.[20] In this study, the growth temperature of 570°C was adopted because it provides the best material quality. It has been used to grow high quality NPN transistors and no abnormal zinc diffusion from base into emitter has been found.[21] Therefore, the observed zinc diffusion from InP emitter to base in the PNP transistor grown by MOCVD in this study was not a direct result of high base growth temperature but rather the inherent higher incorporation efficiency of zinc into InGaAs than into InP.

3. DC Performance of PNP InP/InGaAs HBT Grown by MOCVD

MOCVD-grown InP/InGaAs PNP HBTs were fabricated by using a self-aligned, all wet etch-based process. The p-type metal used in the fabrication was Pt/Ti/Pt/Au and the n-type metal was Ti/Pt/Au. After each p-type metallization, the wafer was annealed at 375°C for 7 s by using rapid thermal annealing (RTA) to improve the ohmic contact.

Figure 2 shows DC common emitter I_C–V_{EC} characteristics of PNP InP/InGaAs HBTs with $1 \times 20\,\mu\mathrm{m}^2$ emitters. The HBTs show strong Early effects as a result of the small base width. The gain increased consequently rapidly as the emitter-collector voltage V_{EC} increased. For example, at $V_{EC} = 3.0\,\mathrm{V}$, $I_B = 0.6\,\mathrm{mA}$, beta of the measured transistor was 28.

However, due to the base push-out, the transistor gain reduced sharply as the collector current/base current increased. Figure 3 illustrates beta as a function of emitter-collector voltage and base current. There are two features noticed, first the gain increased as the emitter-collector voltage increased, for example, at $I_B = 0.6\,\mathrm{mA}$, beta increased from 9.0 at $V_{EC} = 1.5\,\mathrm{V}$ to 28.0 at $V_{EC} = 3.0\,\mathrm{V}$. This is attributed to the small Early voltage due to the thin base. It is also noticed that the gain compressed very rapidly as the base current/collector current increased. As can be seen, beta at $V_{EC} = 3.0\,\mathrm{V}$ decreased from 28 at $I_B = 0.6\,\mathrm{mA}$ to 17.2 at $I_B = 1.2\,\mathrm{mA}$. This shows strong base push-out effects of the PNP InP/InGaAs transistor fabricated and is a direct consequence of the short diffusion length and low transport velocity of the holes.

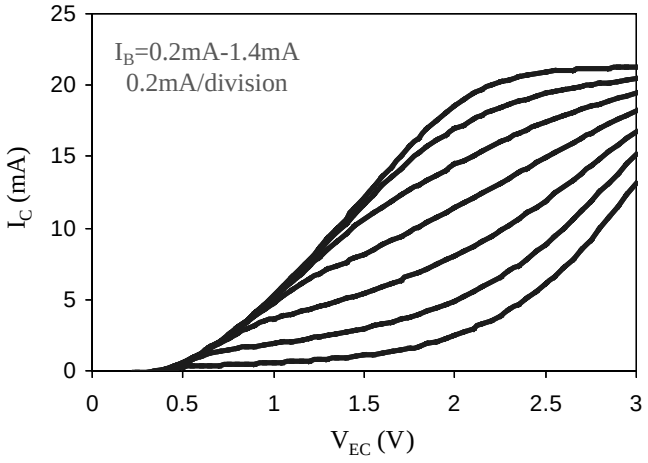

Fig. 2. Common-emitter I_C–V_{EC} characteristics for $1 \times 20\,\mu\mathrm{m}^2$ PNP InP/InGaAs HBT.

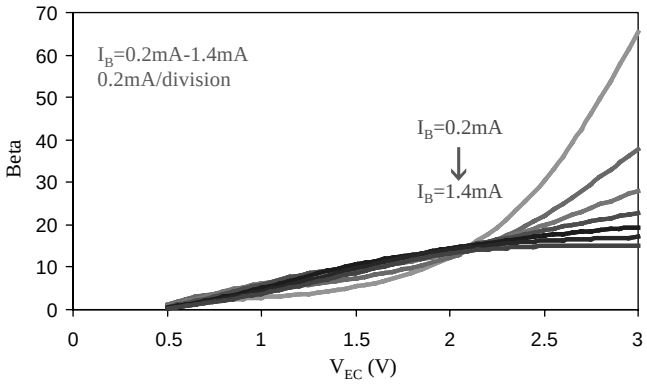

Fig. 3. Beta as a function of V_{EC} and I_B for $1 \times 20\,\mu\mathrm{m}^2$ PNP InP/InGaAs HBT.

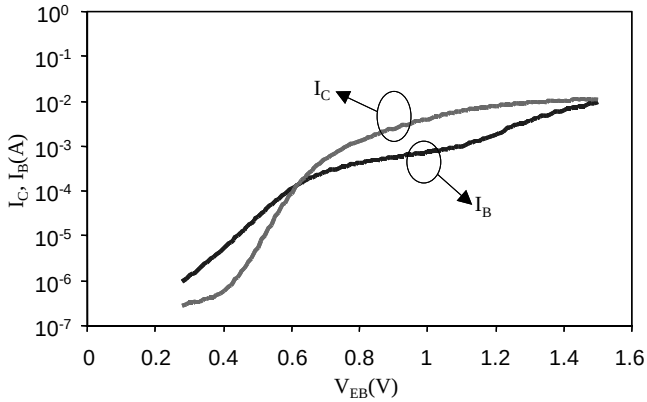

Fig. 4. Gummel plot of $1 \times 20\,\mu\mathrm{m}^2$ PNP InP/InGaAs HBT.

A Gummel plot of $1 \times 20\,\mu\mathrm{m}^2$ PNP InP/InGaAs HBT is shown in Fig. 4. As can be seen, the ideality factors for collector current and base current were 1.3 and 2.5 respectively. The base current is composed of the electrons injected for recombination with holes in the neutral base as well as the electrons back injected across the base-emitter junction. The large base ideality factor suggested that there is considerable amount of recombination in the base-emitter space charge region, the depleted spacer and/or along the external surfaces of the emitter mesa. The device showed considerable presence of base leakage current, which may to a great extent, be introduced by the fact that the band discontinuity appears primarily in the valence band rather than conduction band between InP and InGaAs; the conduction band discontinuity in InP/InGaAs is approximately 200 meV as compared with 400 meV band dis-

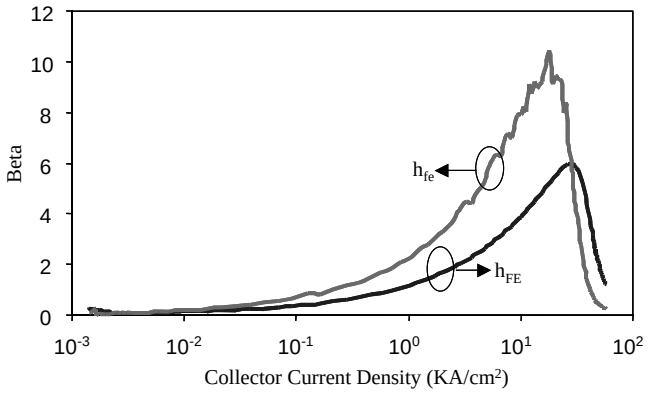

Fig. 5. Current gains as a function of current density for $1 \times 20\,\mu m^2$ PNP InP/InGaAs HBT.

continuity in InAlAs/InGaAs.

Figure 5 shows the current gain as a function of collector current density for PNP InP/InGaAs HBT grown by MOCVD. The differential current gain h_{fe} was larger than large-signal current gain h_{FE} as a result of the larger base current ideality factor than collector current ideality factor according to the following equation:

$$h_{fe} = \frac{\Delta I_C}{\Delta I_B} = \frac{n_B}{n_C} \times \frac{I_C}{I_B} = \frac{n_B}{n_C} \times h_{FE} > h_{FE} \qquad (1)$$

where n_B and n_C are base current and collector current ideality factors respectively.

For example, the peak h_{fe} was 11 while the peak h_{FE} was about 6. Noticed for general Gummel plot measurement, $V_{EC} = V_{EB}$. The current gain could be significantly higher at larger V_{EC} as illustrated in Figs. 2–3. It is also noticed that both differential and large-signal current gain decreased sharply at collector current density larger than 20–30 kA/cm^2. This is due to the significant base push-out when the collector current density exceeds the critical value.

Compared with the previous reported MOMBE-grown PNP InP/InGaAs HBT, lower DC gain (11 versus 20) was observed from the fabricated MOCVD-grown PNP HBT. The reason is most likely due to the lower minority (hole) carrier lifetime in MOCVD grown HBT than that of previously reported MOMBE grown HBT. However, the DC gain value is expected to increase by further optimization of the MOCVD growth conditions and therefore the improvement in material quality.

Figures 6(a) and 6(b) show the Second Ion Mass Spectroscopy (SIMS) results for typical PNP HBTs grown by MOCVD in this work. It is interesting to study the imposed difficulty in growth of this HBT structure and its direct effects on device fabrication and device characteristics. As mentioned above, zinc dopants have relatively high diffusion coefficient and can cause severe degradation in NPN HBT devices. The control of zinc dopant profile is even more critical in case of PNP HBT structures. In a typical InP/InGaAs PNP HBT structure, zinc is used in doping purposes for p^+ InGaAs subcollector, p^- InGaAs collector, P InP emitter, P^+ InP emitter, as well as, p^+ InGaAs emitter cap layer. A variety of issues are involved in growing this structure.

Figure 6(a) shows the profile of the n-type Si-dopant in the MOCVD-grown PNP HBT structure. As can be seen, the n-type dopant was precisely confined in the base layer and the base layer thickness was approximately 500 Å as expected by the design. The n-type doping concentration was about $5 \times 10^{18}\,cm^{-3}$, which was again the design value.

Figure 6(b) shows the zinc dopant profile of the MOCVD-grown PNP HBT. Several features need to be addressed. First, the zinc dopant diffused into the InP substrate from the heavily doped InGaAs subcollector. A zinc dopant tail approximately of 1500 Å was observed to penetrate into the InP substrate. The concentration of zinc dopant ($5 \times 10^{17}\,cm^{-3}$ to $1 \times 10^{18}\,cm^{-3}$) diffused into InP was much lower than that of InGaAs subcollector ($2 \times 10^{19}\,cm^{-3}$). This diffusion from InGaAs subcollector to InP substrate should not affect the device characteristics since the diffused zinc concentration ($5 \times 10^{17}\,cm^{-3}$) was much lower than that of p-type heavily zinc doped InGaAs subcollector ($2 \times 10^{19}\,cm^{-3}$). The diffused zinc dopant depth was also much smaller (~ 1500 Å vs 5000 Å).

The second feature noticed is the doping concentration of zinc-doped p-type InGaAs collector. The lack of double dilution line for DEZn dopants in the present MOCVD system causes a difficulty in obtaining low p-type doing concentration. As a result, the minimum available p-type doping concentration of the MOCVD system used in this work was relatively high ($10^{17}\,cm^{-3}$ to $1 \times 10^{18}\,cm^{-3}$). The MOCVD grown PNP HBT structure in this study employed the lowest doping concentration available and as can be seen from Fig. 6(b), this corresponded to $\sim 1 \times 10^{18}\,cm^{-3}$, which was still about one order of magnitude higher than the desirable collector doping concentration of $5 \times 10^{16}\,cm^{-3}$ to $10^{17}\,cm^{-3}$. The larger than desirable collector doping concentration could cause the increase of base collector capacitance and eventually the degradation of the high speed performance of the PNP HBT, especially f_{max}. A detailed discussion of these issues will be presented later along with the experimental results.

The ideal base-emitter junction of the designed PNP InP/InGaAs HBT structure included a 500 Å n^+ InGaAs base ($5 \times 10^{18}\,cm^{-3}$) followed by 100 Å undoped InGaAs spacer, 1500 Å P InP ($8 \times 10^{17}\,cm^{-3}$) and 700 Å P^+ InP ($2 \times 10^{18}\,cm^{-3}$) emitter. The maximum p-type doping concentration of InP was $2 \times 10^{18}\,cm^{-3}$ because of the relatively low saturation level for p-type material. The SIMS profile shows that the entire InP emitter area was doped at $1 \times 10^{18}\,cm^{-3}$ due to the zinc dopant diffusion and the relatively low saturation level for P-type InP.

Another feature shown in Fig. 6(b) is the zinc dopant pile up on the InGaAs side of the base emitter junction. A 300 Å zinc-doped InGaAs was formed at the base emitter junction due to the zinc diffusion from the InP emitter. The formation of such layer was due to the fact that the zinc incorporation efficiency of InGaAs is 5 to 10 times higher than that of InP. For example, using the same DEZn flow rate of 50sccm, the resulted doping concentration for p-type InGaAs was $1.6 \times 10^{19}\,cm^{-3}$ while it was only $2 \times 10^{18}\,cm^{-3}$ for p-type InP material. The over-saturated zinc dopants were diffused from InP emitter to InGaAs base and spacer. As a result, a zinc-doped InGaAs layer at the base emitter junction was formed.

Based on the results shown in Figs. 6(a) and 6(b) and consideration made above, it is concluded that the "real" base emitter junction structure of MOCVD grown PNP HBTs was as follows: a 300 Å n^+ InGaAs base ($5 \times 10^{18}\,cm^{-3}$) a

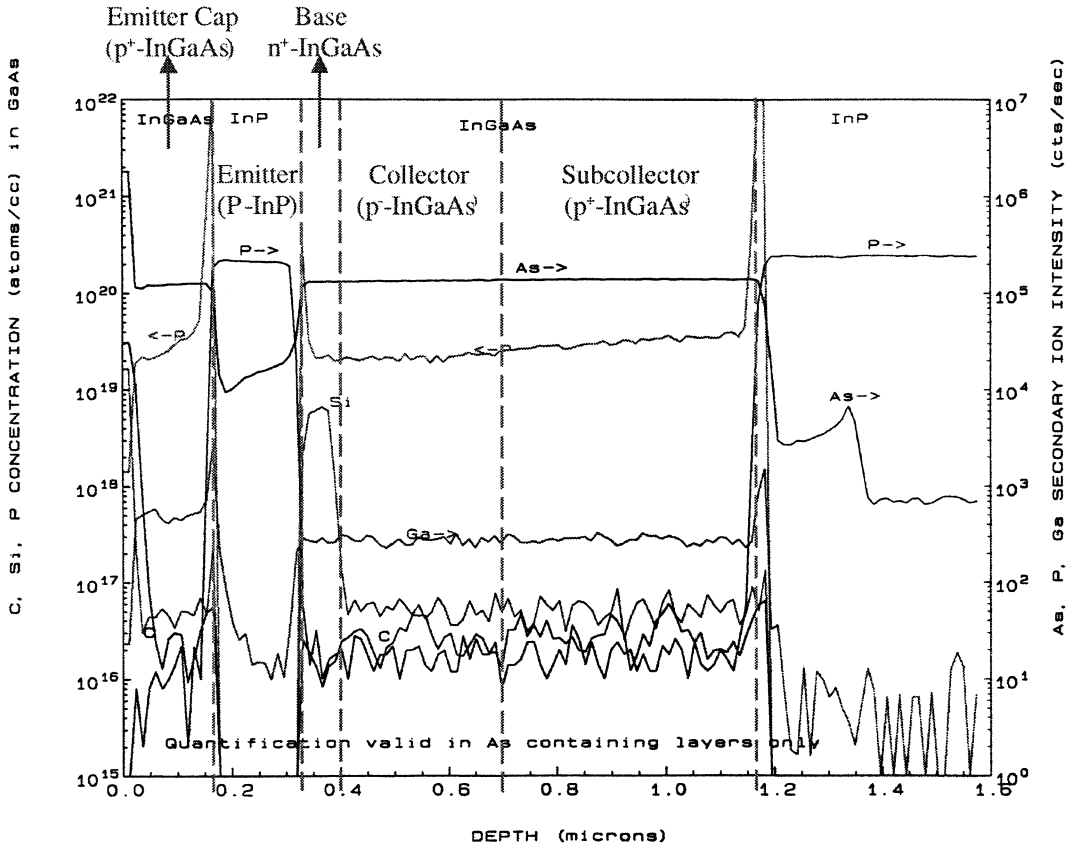

(a)

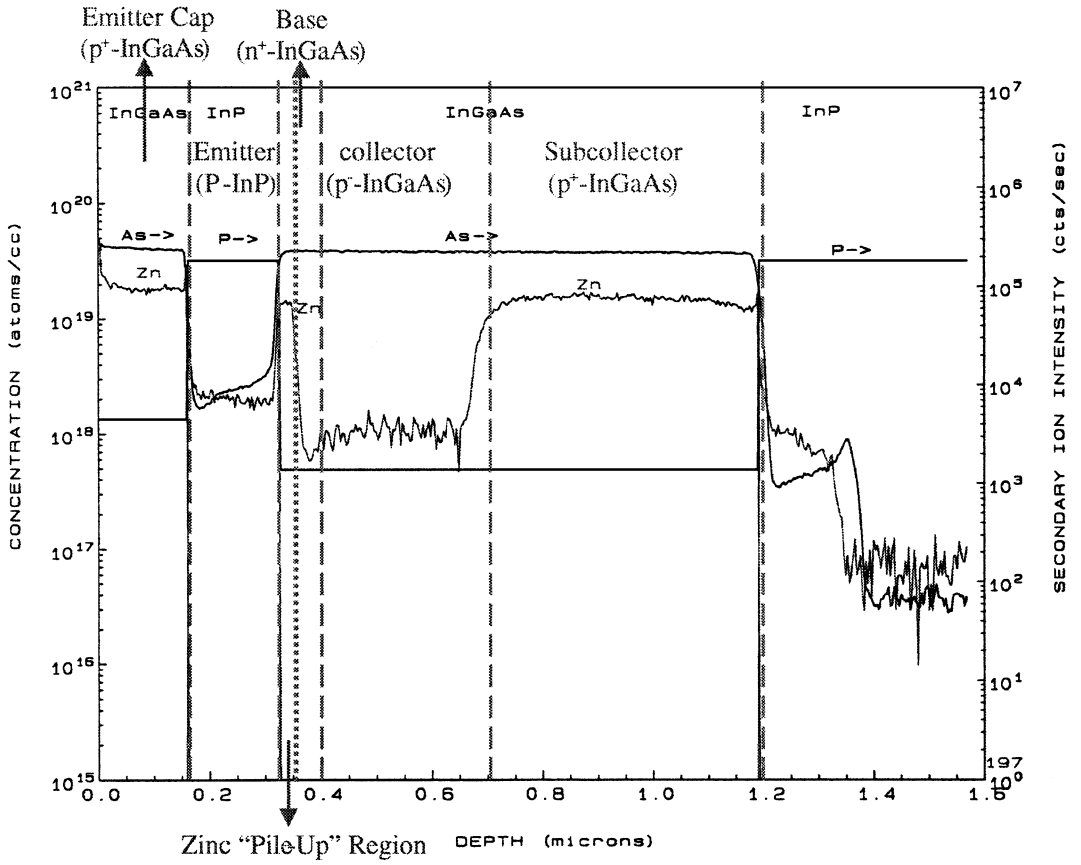

(b)

Fig. 6. (a): SIMS profile for InP/InGaAs PNP HBTs (Si dopant). (b): SIMS profile for InP/InGaAs PNP HBTs (zinc dopant).

300 Å p^+ InGaAs spacer ($\sim$1–1.5 $\times$ 10^{19} cm^{-3}) instead of the initially designed 500 Å n^+ InGaAs base (5×10^{18} cm^{-3}) and 100 Å undoped spacer ($\sim 5 \times 10^{15}$ cm^{-3}). Therefore, the MOCVD grown PNP HBTs shown in Figs. 6(a) and 6(b) had an effective homojunction between the n^+ InGaAs base and the zinc diffusion formed p^+ InGaAs layer. This could consequently lead to lower emitter injection efficiency as well as more base leakage current and recombination.

In order to speculate the effects of the growth profile observed in Figs. 6(a) and 6(b), device simulations were done for two sets of HBT structures. The first one corresponded to the original design as described in Fig. 1. The second one is similar except that the "real" base emitter junction structure was used. The new junction design included a 300 Å n^+ InGaAs base layer and a 300 Å p^+ InGaAs spacer formed by zinc diffusion. A commercially available device simulation tool "MEDICI" was used for the analysis.

The simulated Gummel plots for these two HBTs designs are shown in Fig. 7. As can be seen, the major difference between these two sets of devices was the larger base leakage current for the device with p^+ InGaAs spacer. It is understandable that as the homojunction formed by the p^+ InGaAs spacer and n^+ InGaAs base could not effectively block the electrons, higher back injection current could be present due to the lack of bandgap discontinuity at the conduction band. As a result, the base leakage current was higher and the emitter injection efficiency was reduced, especially at low V_{BE} biasing voltage.

To solve this problem, two approaches could be adopted. The first one is to increase the spacer width. A larger spacer, such as 200 Å instead of 100 Å could be employed to reduce the DEZn diffusion into the n^+ InGaAs base. The second one involves significant decrease of DEZn flow during the growth of the InP emitter. However, a decrease of the InP emitter doping concentration could also reduce the current gain of the HBT devices. Moreover, in order to reduce the collector doping concentration, the MOCVD system used in this work has to be modified to include double dilution lines for the DEZn precursor. A much larger dynamic range could be obtained using such approach than using the current approach, which employs a single gas line for the DEZn precursor. For example, a doping concentration range of 5×10^{16} cm^{-3} to 2×10^{19} cm^{-3} could be achieved by reconfiguring the single line to double dilution line for DEZn precursor, which corresponds to a dynamic range of 400.

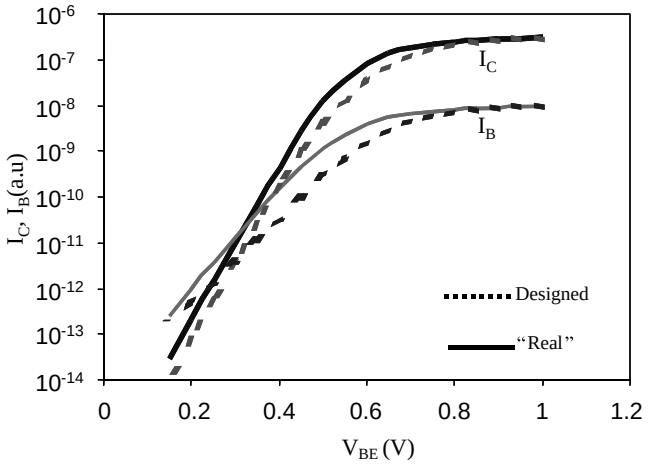

Fig. 7. Simulated Gummel plots for HBTs with p^+ InGaAs spacer ("real") and with undoped InGaAs spacer (designed).

4. Microwave Performance of InP/InGaAs PNP HBT Grown by MOCVD

Small signal S-parameters were measured using an HP8510B network analyzer and coplanar probes from 0.5 GHz to 25.5 GHz. Figure 8 shows the microwave performance of a $1 \times 20\,\mu m^2$ HBT biased at $V_{EC} = 3.0$ V and $I_C = 16.6$ mA. f_T and f_{max} were found to be 11.2 GHz and 8.1 GHz respectively. While the f_T performance compares with that of similar designs grown by MOMBE (f_T of 10.5 GHz[17]), the f_{max} was considerably lower (f_{max} of 25 GHz[17]). This is due to the limitation of minimum controllable p-type doping concentration in the MOCVD system used for growth of these device layers. (minimum p-doping concentration of 1×10^{18} cm^{-3} was possible in this system instead of the desirable value of 10^{16}–10^{17} cm^{-3} for collector doping).

As a result, the base-collector capacitance C_{BC} was high and the f_{max} performance was degraded considerably. For example, the collector doping concentration in the present HBT structure was about one order of magnitude higher than the desired value (1×10^{18} versus 5×10^{16} cm^{-3} -1×10^{17} cm^{-3}). This contributes to almost 10 times larger C_{BC} than the HBT with the desired low collector doping concentration. It is well known that the maximum frequency of oscillation f_{max} is inversely proportional to square root of C_{BC}. As a result, an almost three times ($\sqrt{10} = \sim 3$) degradation in f_{max} was observed (8.1 GHz versus 25 GHz). Further improvement in f_{max} performance is expected to be feasible by controlling the doping concentration of the collector.

From the f_T and f_{max} measurements, the sum of base transit time and the collector charging time can be extrapolated.[22] The total emitter-to-collector delay τ_{ec} is:

$$\tau_{ec} = \frac{1}{2\pi f_T} = \tau_e + \tau_b + \tau_{pcd} + \tau_c$$
$$= \frac{kT}{qI_E} C_{BE} + \left(\frac{W_B^2}{2D_p} + \frac{W_B}{2v_{bc}} \right)$$
$$+ \frac{W_c}{2v_C} + \left(R_C + R_E + \frac{kT}{qI_E} \right) C_{BC}$$

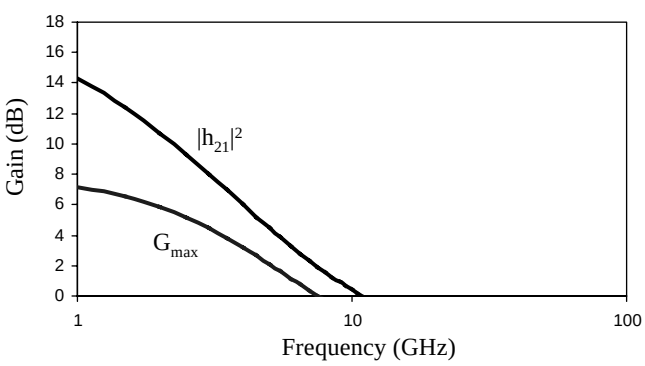

Fig. 8. Microwave performance of $1 \times 20\,\mu m^2$ PNP InP/InGaAs HBT.

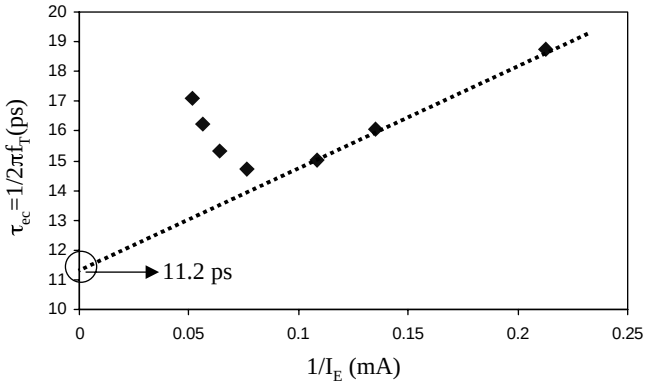

Fig. 9. τ_{ec} as a function of the reciprocal of emitter current for PNP InP/InGaAs HBT grown by MOCVD.

$$= \frac{1}{I_E}\left(\frac{kT}{q}C_{BE} + \frac{kT}{q}C_{BC}\right) + \left[\left(\frac{W_B^2}{2D_p} + \frac{W_B}{2v_{bc}}\right) + \frac{W_c}{2v_c} + (R_c + R_E)\,C_{BC}\right] \quad (2)$$

where τ_e, τ_b, τ_{pcd}, and τ_c are the emitter charging, base transit, pre-collector delay, and collector charging times; W_B is the neutral base width; W_C is the collector depletion width; v_{bc} is the velocity with which electrons are swept into the base collector depletion region; v_c is the average electron velocity in the collector.

Figure 9 shows the total transit time from emitter to collector τ_{ec} as a function of the reciprocal of the emitter current for a $1 \times 20\,\mu m^2$ PNP HBT with $V_{EC} = 2.4$ V. One can see that τ_{ec} follows the linear relationship with $1/I_E$ at low current levels. At high current levels, due to the Kirk effects, the effective W_B and C_{BC} increase and therefore τ_{ec} increases as a result.

By extrapolating the region where τ_{ec} follows linear relationship with $1/I_E$, one can find τ' at $1/I_E = 0$,

$$\tau' = \left(\frac{W_B^2}{2D_p} + \frac{W_B}{v_{bc}}\right) + \frac{W_c}{2v_c} + (R_c + R_E)C_{BC} \quad (3)$$

while Q_d, the slope of the curve, is given by:

$$Q_d = \frac{kT}{q}C_{BE} + \frac{kT}{q}C_{BC} \quad (4)$$

The sum of base transit time and the collector charging time τ' at $1/I_E = 0$ was found to be 11.2 ps. This almost accounts for 75% of the total emitter to collector delay time which was 15.0 ps under the biasing condition of $I_E = 9.2$ mA. It indicates that the base transit time and the collector charging time dominate the high frequency performance of the InP/InGaAs PNP transistor, while other components such as emitter charging time and pre-collector delay time only account for 25% of the total emitter to collector delay time.

The above results indicate that the high frequency performance of InP/InGaAs PNP HBTs is to a great extent limited by the use of uniformly doped InGaAs base. Compositionally graded base[23] and doping graded base designs[24] have been employed in AlGaAs/GaAs material system to improve the high speed performance of the PNP AlGaAs/GaAs HBTs. Similar approaches can be applied to InP/InGaAs PNP HBTs, where the introduction of electrical fields into the n-type base region could aid the hole transition through the base and reduce the total emitter to collector transit time significantly.

Improvement is also expected by decreasing the collector doping concentration as for example obtained by lowering the minimum controllable p-type doping concentration from high $10^{17}\,cm^{-3}$ to $10^{16}\,cm^{-3}$.[17] Although this approach will severe the base-push out (Kirk effects), it could reduce the base-collector capacitance by increasing the collector depletion width. As a result, the f_{max} performance could be improved significantly over the present characteristics, which are limited by the lowest controllable p-type doping concentration of the present growth system.

5. Conclusion

PNP InP/InGaAs HBTs have been grown by MOCVD for the first time and successful operation of these HBTs was demonstrated. Gain of more than 10, f_T of 11.2 GHz and f_{max} of 8.1 GHz have been achieved by a $1 \times 20\,\mu m^2$ HBT. While the cut-off frequency performance f_T was comparable with state-of-art results for InP/InGaAs PNP HBTs grown by MOMBE, f_{max} was found to be lower. Growth limitations in terms of the lowest achievable p-type doping concentration for collector design are responsible for the observed differences. Furthermore, a zinc pile up layer on the InGaAs side of the base emitter junction was observed due to the zinc diffusion from the InP emitter. The formation of such layer was due to the fact that the zinc incorporation efficiency of InGaAs is 5 to 10 times higher than that of InP. The zinc pile up layer increased the base leakage current and decreased the emitter injection efficiency. These phenomena were confirmed by the reported device simulation results. Finally, characterization of the fabricated devices shows that the base transit time and collector charging time dominate the high frequency performance of PNP InP/InGaAs HBT.

Acknowledgement

This work is supported by ARO MURI (DAAH04-96-1-0001).

1) Y. Matsuoka, S. Yamahata, K. Kurishima and H. Ito: Jpn. J. Appl. Phys. **35** (1996) 5646.
2) H. Masuda, K. Ouchi, A. Terano, H. Suzuki, K. Watanabe, T. Oka, H. Matsubara and T. Tanoue: GaAs IC Symp Tech. Dig. (1997) 139.
3) H.-F Chau and Y.-C Kao: Int. Electron. Device Meet. Tech. Dig. (1993) p. 783.
4) S. Yamahata, K. Krishima, H. Nakajima, T. Kobayashi and Y. Masuoka: GaAs IC Symp Tech Dig. (1994) 345.
5) Y. Matsuoka, H. Nakajima, K. Kurishima, T. Kobayashi, M. Yoneyama and E. Sano: 6th Int Conf. On InP and Related Materials, (1994) p. 555.
6) K. Kurishima, H. Nakajima, S. Yamahata, T. Kobayashi and Y. Matsuoka: IEICE Trans. Electron. **E78-C** (1995) 1171.
7) S. Blayac, M. Riet, J. L. Benchimol, P. Berdaugher, N. Kauffman, J. Godin and A. Scavennec: 2000 Int Conf on Indium Phosphide and Related Materials (2000) 481.
8) D. Pavlidis, D. Sawdai and D. Cui: Proc. SPIE **3861** (1999) 11.
9) D. Sawdai and D. Pavlidis: Topical Workshop on Heterostructure Microelectronics for Information Systems Applications (Kanagawa, Japan, Aug. 30–Sept. 2, 1998). proceedings to appear in J. Solid-State Electronics.
10) D. Sawdai and D. Pavlidis: IEEE Trans. Microwave Theory & Techniq. **47** (2000) 1439.
11) D. Slater, P. Enquist, J. Hutchby, A. Morris and R. Trew: IEEE Electron Device Lett. **25** (1994) 92.

12) D. Sawdai, X. Zhang, D. Pavlidis and P. Bhattacharya: 1998 Int Conf InP and Related Materials (1998) 72.
13) D. Sawdai, X. Zhang, D. Cui, D. Pavlidis and P. Bhattacharya: 1999 Int Conf InP and Related Materials (1999) p. 187.
14) T. Won, C. Peng, J. Chyi and H. Morkoc: IEEE Electron Device Lett. **9** (1988) 334.
15) A. Nakagawa and K. Inoue: IEEE Electron Device Lett. **13** (1992) 285.
16) W. Stanchina, R. Metzgerm, M. Pierce, J. Jensen, L. McCray, R. Wong-Quen and F. Williams: 1993 Int Conf InP and Related Materials (1993) p. 569.
17) L. M. Lunardi, S. Chandrasekhar and R. A. Hamm: IEEE Electron Device Lett. **14** (1993) 19.
18) D. Cui, H. S. Hsu and D. Pavlidis: 13th Int. Conf. Indium Phosphide and Related Materials, May14–18, 2001, Nara, Japan.
19) R. Bhat, M. A. Koza, J. I. Song, S. A. Schwarz, C. Caneau and W. P. Hong: Appl. Phys. Lett. **65** (1994) 338.
20) K. Kurishima, T. Kobayashi, H. Ito and U. Gosele: J. Appl. Phys. **79** (1996) 4017.
21) D. Sawdai, J.-O. Plouchart, D. Pavlidis, A. Samelis and K. Hong: 1996 Int Conf InP and Related Materials (1996) 133.
22) D. Slater, P. Enquist, F. Najjar, M. Chen, J. Hutchby, A. Morris and R. Trew: IEEE Electron. Device Lett. **12** (1991) 54.
23) A. Kameyama, A. Massengale, C. Dai and J. Harris: IEICE Trans. Electron. **E79-C** (1996) 518.
24) D. Hill, T. S. Kim and H. Q. Tseng: IEEE Electron Device Lett. **14** (1993) 185.